IOP PUBLISHING PHYSICS IN MEDICINE AND BIOLOGY

Phys. Med. Biol. **52** (2007) 7007–7022 doi:10.1088/0031-9155/52/23/016

Modelling the electrical properties of tissue as a porous medium

S W Smye[1], C J Evans[1], M P Robinson[2] and B D Sleeman[3]

[1] Department of Medical Physics and Engineering, Leeds Teaching Hospitals, St James's University Hospital, Leeds LS9 7TF, UK
[2] Department of Electronics, University of York, Heslington, York YO10 5DD, UK
[3] Department of Applied Mathematics, University of Leeds, Leeds LS2 9JT, UK

E-mail: SWSmye@leeds.ac.uk

Received 29 June 2007, in final form 27 September 2007
Published 12 November 2007
Online at stacks.iop.org/PMB/52/7007

Abstract

Models of the electrical properties of biological tissue have been the subject of many studies. These models have sought to explain aspects of the dielectric dispersion of tissue. This paper develops a mathematical model of the complex permittivity of tissue as a function of frequency f, in the range $10^4 < f < 10^7$ Hz, which is derived from a formulation used to describe the complex permittivity of porous media. The model introduces two parameters, porosity and percolation probability, to the description of the electrical properties of any tissue which comprises a random arrangement of cells. The complex permittivity for a plausible porosity and percolation probability distribution is calculated and compared with the published measured electrical properties of liver tissue. Broad agreement with the experimental data is noted. It is suggested that future detailed experimental measurements should be undertaken to validate the model. The model may be a more convenient method of parameterizing the electrical properties of biological tissue and subsequent measurement of these parameters in a range of tissues may yield information of biological and clinical significance.

(Some figures in this article are in colour only in the electronic version)

1. Introduction

The electrical properties of tissue have been studied for many years (Foster and Schwan 1989). These properties are conveniently described using the absolute complex permittivity ε, which comprises the permittivity ε' (describing the polarizability of the medium) and conductivity σ. The absolute complex permittivity is then defined by

$$\varepsilon = \varepsilon' + \mathrm{i}\frac{\sigma}{\omega}$$

where ω is the angular frequency of the applied electrical field. Conventionally, the complex permittivity is expressed relative to the permittivity of free space, ε_0, and thus

$$\varepsilon = \varepsilon' + \mathrm{i}\frac{\sigma}{\omega\varepsilon_0} \tag{1}$$

where it is understood that ε' now denotes relative permittivity and σ denotes absolute conductivity and is in units of S m^{-1}.

A variety of approaches have been taken to describing the dispersion relationship (Foster and Schwan 1989, Raicu 1999, Paulson *et al* 2000), including use of semi-empirical expressions (Cole and Cole 1941) and those based on theoretical analysis (for example, see MacDonald (1987)). However, only limited insight into the link between the underlying structural features and the consequent electrical properties of tissues has been gained. For example, the framework developed by Hanai *et al* (1979), and applied by others to biological tissues (Foster and Schwan 1989), treats tissue as a suspension of uniform spheres in a conducting medium. The geometrical accuracy of this model is therefore limited. Other investigators have adapted this basic model by considering the suspensions as ellipsoidal particles (Boned and Peyrelasse 1983). Gielen and co-workers (Gielen *et al* 1986) developed a model of electrical conduction in skeletal muscle based on a particular geometry for tissue structure, in which muscle cells were considered as tubes with uniform hexagonal cross-section. However, the problem of characterizing the complex geometry of tissue in a convenient manner remains.

Sahimi (2003) has noted that the enormous variation in the morphology of natural or man-made materials made the task of describing and quantifying such morphologies appear hopeless, until a few decades ago. A number of recent developments have changed this outlook, including novel experimental techniques, advances in computational power and the concepts of fractal geometry and percolation theory. For example, Dissado and co-workers (Dissado 1990) have developed a fractal approach to the description of tissue permittivity. However, in general, such newer techniques have not been widely applied to the description of the electrical properties of tissue. This paper develops a mathematical framework based on percolation theory.

The frequency dependence of the complex permittivity of biological tissue in the so-called β-dispersion is attributed to capacitive charging of cellular membranes and dipolar relaxation of proteins. It has a typical centre frequency of 3 MHz (Foster and Schwan 1989) and is the dispersion of interest in this paper. The general approach to describing the dispersion has been to assume initially that a single dipole relaxation time τ characterizes the particular polarization process (the Debye model; Pethig and Kell 1987).

$$\varepsilon = \varepsilon_\infty + \frac{\varepsilon_\mathrm{s} - \varepsilon_\infty}{1 - \mathrm{i}\omega\tau}$$

where ε_∞ and ε_s denote the complex permittivities when $\omega\tau \gg 1$ and $\ll 1$, respectively. The likely distribution of relaxation times is then accounted for by an empirical parameter, most commonly by using the expression developed by Cole and Cole (1941), which introduces a distribution parameter α:

$$\varepsilon = \varepsilon_\infty + \frac{\varepsilon_\mathrm{s} - \varepsilon_\infty}{1 + (-\mathrm{i}\omega\tau)^{1-\alpha}},$$

τ becomes, in effect, an average relaxation time for the tissue in the frequency range of interest. Empirically, the relative permittivity spectrum of a tissue may therefore be described in terms of a sum of multiple terms similar to that above as

$$\varepsilon(\omega) = \varepsilon_\infty + \sum_n \frac{\Delta\varepsilon_n}{1 + (-\mathrm{i}\omega\tau_n)^{1-\alpha_n}} + \frac{\mathrm{i}\sigma_\mathrm{s}}{\omega\varepsilon_0} \tag{2}$$

where $\Delta\varepsilon_n = \varepsilon_s - \varepsilon_\infty$ for each (the nth) term and σ_s denotes the static ionic conductivity (Gabriel *et al* 1996a). It is important to note that the choice of the number of terms is dependent on the degree of accuracy sought, reflecting the empirical nature of the curve fit. Gabriel *et al* (1996a) note that $n = 4$ or 5 are common choices, and to fit to the β-dispersion, two terms ($n = 2$ and 3) are used in a four-term model (Gabriel *et al* 1996a).

The question to be answered may be posed as follows: can the expression for $\varepsilon(\omega)$ covering the β-dispersion—assumed to cover the frequency range 100 kHz to 10 MHz—be deduced from the geometry of the tissue using parameters that reflect cellular arrangements? A similar issue has been of long standing interest in geophysics (Haslund *et al* 1994) and materials physics (Feldman *et al* 2002, Sahimi 2003, Wilkinson *et al* 1983): in porous rock containing water and/or oil, measurements of $\varepsilon(\omega)$ are undertaken in an attempt to determine the extent of oil deposits. The problem is to determine the relationships between the properties of the composite material, the properties of its constituents and their relative presence in the composite. This is similar to the goal of tissue impedance measurements, which seeks to determine tissue composition. Tissue comprises cells, with spaces between the cells, and may therefore, in some general sense, be likened to a porous medium. The parameters of interest include the relative volumes of the cells and the extra cellular space.

This paper applies a mathematical model to the description of the electrical properties of tissue, which enables $\varepsilon(\omega)$ to be calculated given knowledge of the structural parameters of a porous medium. The model was originally developed by Hilfer (1991) and provides an alternative, possibly more flexible, approach to the characterization of the electrical properties of tissue. It is applied to the description of the electrical properties of liver tissue in the β-dispersion, and compared with experimental measurements from previous work by Gabriel *et al* (1996b). The analysis may permit novel parameters for some tissues (those which have random arrangements of cells), notably the porosity of the underlying cellular structure, to be measured, which may be of clinical significance. Possible applications of the model may include describing the electrical properties of malignant tissue (Walker *et al* 2000), which tends to be poorly differentiated and have a relatively random cellular structure. Another possible application may be modelling the behaviour of tissue in which changes in the water content (which may occur during dialysis, for example Bradbury *et al* (2001)) affected the porosity.

2. Development of model

The foundations of the model are described by Hilfer (1991) and Hilfer and Haslund (Haslund *et al* 1994). The starting point for application of this model to tissue is the assumption that tissue comprises a collection of unit cells. As is explained below, these unit cells may or may not correspond to biological cells and are defined as having a length scale L. It is assumed that these unit cells are arranged at random and that the spaces between the unit cells (the pores in Hilfer's original description) are occupied by a conducting (and, in this paper, polarizable) medium. The porosity ϕ of the tissue is then defined as the volume of the pore space divided by the total volume. The length scale L is defined such that L^3 is the smallest volume of measurement. In this paper, L is assumed to be of the order of a cellular length, but may equally be of the length scale of a structural group of cells, or even at a sub-cellular level, depending on the tissue structure being modelled. The significance of L is that a local porosity at position $\mathbf{R}$ within the tissue may be defined as taking the value $\phi(\mathbf{R}, L)$ within the unit cell and that the properties of adjacent unit cells are not correlated. A local porosity probability distribution function $\mu(\phi, \mathbf{R}; L)$ is then defined such that $\mu(\phi, \mathbf{R}; L)\,\mathrm{d}\phi$ is the probability of finding the local porosity ϕ in the range ϕ to $\phi + \mathrm{d}\phi$ in a volume element of linear dimension

L at the point **R**. If the tissue is homogeneous, then μ must be independent of **R** and the bulk porosity $\bar{\phi}$ is given by

$$\bar{\phi} = \int_0^1 \phi \mu(\phi; L)\, \mathrm{d}\phi.$$

The second parameter chosen to characterize local geometry is whether the space between the cells percolates or not. For a comprehensive discussion of percolation, see Sahimi (2003). For cubic volume elements, each element is classified as percolating or non-percolating according to whether or not there exists at least one face of the cube which can be connected to any of the other faces via a path contoured completely inside the pore space. A function $\lambda(\phi)$ is defined which denotes the fraction of percolating elements with local porosity ϕ. The geometry of the tissue on a length scale of L is thus characterized by the two parameters μ and λ.

Because all volume elements are statistically independent, standard effective medium theory (Landauer 1978, Sahimi 2003) may be employed to write a self-consistency equation for the effective complex permittivity ε of the medium (see Sahimi 2003):

$$\int_g \frac{\varepsilon_{\mathrm{loc}} - \varepsilon}{\varepsilon_{\mathrm{loc}} + 2\varepsilon}\, \mathrm{d}p(g) = 0 \tag{3}$$

where $\varepsilon_{\mathrm{loc}}$ is the local effective complex permttivity, g denotes the local geometry and the probability measure $p(g)$ represents the statistical distribution of local complex permittivities. $p(g)$ is not usually known and $\mu(\phi)$ and $\lambda(\phi)$ are used as approximate descriptions. In this case, $\varepsilon_{\mathrm{loc}}$ is replaced by an approximate effective permittivity, which depends only on the local porosity ϕ, and is described in terms of percolating and non-percolating elements.

If $\varepsilon_{\mathrm{C}}(\omega, \phi)$ and $\varepsilon_{\mathrm{B}}(\omega, \phi)$ denote the local effective permittivities for conducting (percolating) and blocking (non-percolating) volume elements respectively, then equation (3) gives

$$\int_0^1 \frac{\varepsilon_{\mathrm{C}} - \varepsilon}{\varepsilon_{\mathrm{C}} + 2\varepsilon} \lambda\mu\, \mathrm{d}\phi + \int_0^1 \frac{\varepsilon_{\mathrm{B}} - \varepsilon}{\varepsilon_{\mathrm{B}} + 2\varepsilon} (1 - \lambda)\mu\, \mathrm{d}\phi = 0. \tag{4}$$

Equation (4) represents the basic description of the tissue and this analysis solves the forward problem by calculating ε for given λ, μ. Note that ε is not a function of the local porosity ϕ.

In summary, the model describes the complex permittivity of a tissue as a weighted spatial average of the separate permittivities of conducting and blocking elements. The primary purpose of the paper is to develop the theoretical framework for ε, but an outline of how the parameters λ, μ and ϕ might be measured from histological observations is given (see also appendix A).

The tissue chosen for analysis must conform to the assumptions made so far, including a random orientation of unit cells and a combination of blocking and conducting geometries. A number of tissues in which these assumptions may hold include poorly-differentiated tumours, adipose tissue, bone marrow, bone (between lamellae) and liver lobules (Cormack 2001). Liver tissue (Cormack 2001) comprises lobules, which are bounded by fibrous septa enclosing roughly hexagonal areas of hepatocytes (the functional liver cells). Observed under relatively low microscopic power, within each lobule, irregular rows of hepatocytes radiate towards a central vein (see figure 1). Between each row, lie narrow spaces called sinusoids. The hepatocytes make up irregular curved perforated plates that constitute a three-dimensional sponge-work, the interstices of which are filled with blood, thereby exposing much of the cell surface to blood (see figure 2). The histological analysis identifies the cells as arranged in an approximately random, plate-like, configuration. In principle then, λ and μ may be measured from micrographic images of tissue sections and an approach to doing this for liver tissue is set

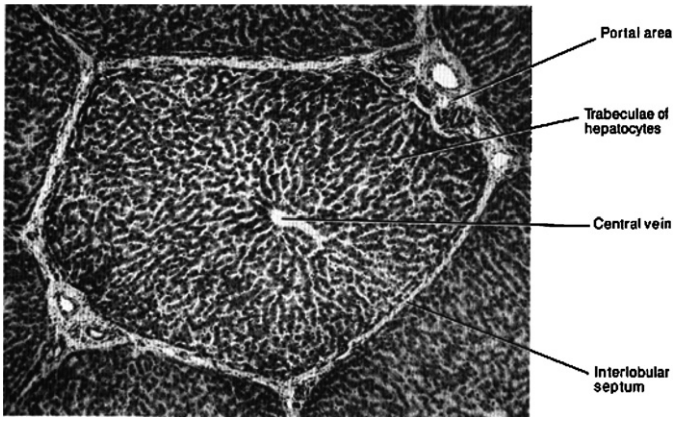

Figure 1. Liver lobule outlined by fibrous septa in pig liver. From figure 13–18 in *Essential Histology* (Cormack 2001) and reproduced with kind permission of the publishers (JB Lippincott Company) and the author. In human tissue, lobules are typically of size 1000–2000 μm (Leeson and Leeson 1981a).

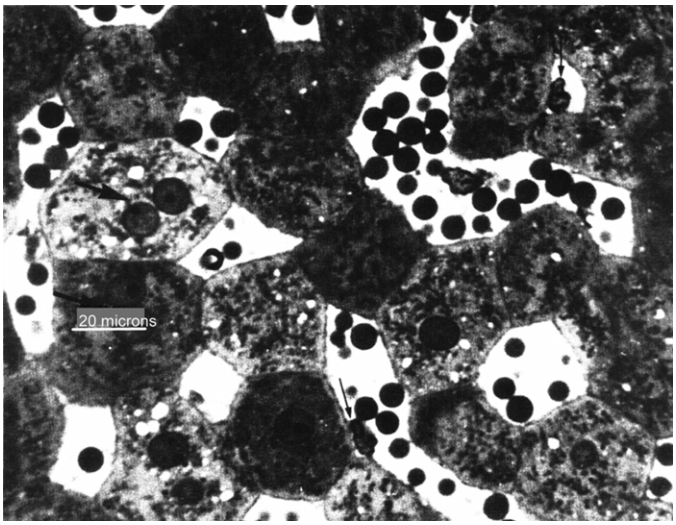

Figure 2. Structure of liver lobule, showing liver cells (dark) and intercellular spaces (light). Red blood cells are also seen within the spaces (dark circles). From figures 11–61 in *Histology* (Leeson and Leeson 1981b) and reproduced with kind permission of the publishers, Elsevier. Approximate scale bar added.

out in more detail in appendix A. The purpose of this paper is to offer a proof-of-principle over the frequency range considered, rather than a detailed assessment of quantitative agreement and it is assumed that μ is a 'top-hat' function of ϕ, centred on a value ϕ_0 and of width 2Δ (<1). Thus,

$$\begin{aligned} \mu(\phi) &= 0 \quad && \phi < \phi_0 - \Delta \\ &= \mu_0 \quad && \phi_0 - \Delta < \phi < \phi_0 + \Delta \\ &= 0 \quad && \phi > \phi_0 + \Delta. \end{aligned} \tag{5}$$

Since

$$\int_0^1 \mu(\phi)\,\mathrm{d}\phi = 1$$

then

$$\mu_0 = 1/2\Delta. \tag{6}$$

Also, from equations (5) and (6), the mean porosity is given by

$$\begin{aligned}\bar{\phi} &= \int_0^1 \phi\mu(\phi)\,\mathrm{d}\phi \\ &= \phi_0,\end{aligned} \tag{7}$$

$\lambda(\phi)$ is the fraction of percolating cells with local porosity ϕ. Again, given that the aim of this paper is to offer a theoretical framework, which might be more rigorously tested subsequently using extensive experimental data, a simple approach is adopted and it is assumed that

$$\begin{aligned}\lambda(\phi) &= 0 \quad 0 < \phi < \phi_\mathrm{p} \\ &= 1 \quad \phi_\mathrm{p} < \phi < 1.\end{aligned} \tag{8}$$

This implies that there is a critical porosity ϕ_p such that above this value all elements percolate. This is the so-called grain-consolidation model (Hilfer 1991). It is also assumed that

$$\phi_0 - \Delta < \phi_\mathrm{p} < \phi_0 + \Delta. \tag{9}$$

From equations (4)–(9)

$$\frac{2\Delta}{3\varepsilon} = \int_{\phi_\mathrm{p}}^{\phi_0+\Delta} \left\{\frac{\mathrm{d}\phi}{\varepsilon_\mathrm{c} + 2\varepsilon}\right\} + \int_{\phi_0-\Delta}^{\phi_\mathrm{p}} \frac{\mathrm{d}\phi}{\varepsilon_\mathrm{B} + 2\varepsilon}. \tag{10}$$

The forms for ε_C, ε_B may also be estimated from histological observations (see figure 2); here, it is assumed that conducting local geometries in the liver tissue may be represented by a layer of cellular material of cross-sectional area a and complex permittivity $\varepsilon_{\mathrm{cell},}$ in parallel with a layer of extracellular fluid (ecf) which has complex permittivity ε_ecf. This configuration may be thought of as being arranged between the capacitor plates of spacing D and cross-sectional area A (see figure 3). For blocking geometries, a plate of cellular material of thickness d is arranged between the plates in series with a layer of ecf (see figure 3). The effect of the interlobular fibrous septa is neglected. Analysis based on figure 3 then gives

$$\varepsilon_\mathrm{C} = \varepsilon_\mathrm{cell}(1-\phi) + \phi\varepsilon_\mathrm{ecf} \tag{11}$$

and

$$\varepsilon_\mathrm{B} = \frac{\varepsilon_\mathrm{cell}\varepsilon_\mathrm{ecf}}{\varepsilon_\mathrm{ecf}(1-\phi) + \phi\varepsilon_\mathrm{cell}} \tag{12}$$

as $\phi = 1 - (a/A)$ for the conducting geometry and $\phi = 1 - (d/\mathrm{D})$ for the blocking geometry. The forms for $\varepsilon_\mathrm{cell}$ and ε_ecf need to be described using observations of the cellular structure. This is detailed in appendix B, based on a simple cubic cellular geometry of with cubes of side t, but different geometries will yield different forms for ε_C, $\varepsilon_{\mathrm{B},}$ and $\varepsilon_\mathrm{cell}$. From appendix B and some further algebraic manipulation, $\varepsilon_\mathrm{cell}$ and ε_ecf may be written in the form

$$\varepsilon_\mathrm{cell} = a + \mathrm{i}b \qquad \varepsilon_\mathrm{ecf} = c + \mathrm{i}h \tag{13}$$

where

$$\begin{aligned}a &= \{c(1+\eta c) + \eta h^2\}/\{(1+\eta c)^2 + \eta^2 h^2\} \\ b &= h/\{(1+\eta c)^2 + \eta^2 h^2\} \\ c &= \varepsilon'_\mathrm{ecf} \\ h &= \sigma_\mathrm{ecf}/2\pi f\varepsilon_0 \\ \eta &= 2\varepsilon_0/C_\mathrm{m}t\end{aligned}$$

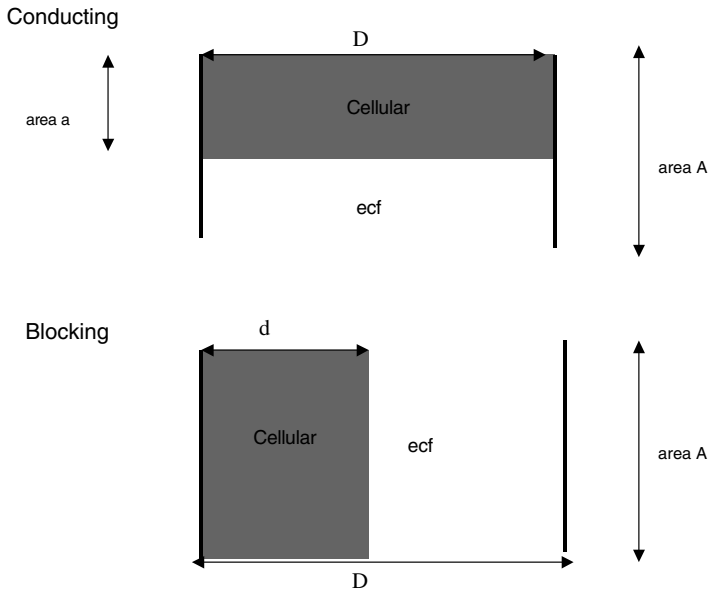

Figure 3. Conducting and blocking geometries

and C_m denotes the cell membrane capacitance per unit area. Re-stating equation (1)

$$\varepsilon = \varepsilon' + \mathrm{i}\frac{\sigma}{\omega\varepsilon_0}.$$

From equations (1), (10) and (13), after some algebraic manipulation, the dispersion relationship $\varepsilon(\omega)$ is given implicitly by

$$\frac{2\Delta}{3\varepsilon} = \int_{\phi_p}^{\phi_0+\Delta} \frac{X^* + \phi Y^*}{E(\phi)}\,\mathrm{d}\phi + \int_{\phi_0-\Delta}^{\phi_p} \frac{\varepsilon_{ecf} - \phi Y}{\varepsilon_{ecf} X - 2\varepsilon\phi Y}\,\mathrm{d}\phi \tag{14}$$

where

$$X = a + \mathrm{i}b + 2\varepsilon$$

$$Y = c - a + \mathrm{i}(h - b)$$

$$E(\phi) = XX^* + (Y^*X + X^*Y)\phi + YY^*\phi^2$$

and X^*, Y^* denote the complex conjugates of X and Y. Each of the integrals on the RHS of equation (14) may be evaluated analytically, and the resulting equation then solved numerically using Maple 10 (Waterloo Maple Inc.) for the absolute conductivity σ and the relative permittivity ε' of the tissue for $10^4 < f < 10^7$ Hz. The results are compared to an empirical fit given by equation (2). The choice of parameter values is now described.

3. Parameter values for model

The estimates of the parameter values used in the solution of equation (14) are given in table 1, together with the source of each estimate or parameter range. These parameters are estimates and future work might focus on more accurate experimental measurements, including those

Table 1. Estimates of model parameters.

Model parameter	Estimate or range	Source of estimate
$\varepsilon'_{\mathrm{cyt}}$, $\varepsilon'_{\mathrm{ecf}}$	80	Foster and Schwan (1987)
σ_{cyt}	0.3 S m^{-1}	Gowrishanker and Weaver (2006)
σ_{ecf}	1.2 S m^{-1}	Gowrishanker and Weaver (2006)
C_{m}	0.01 F m^{-2}	Foster and Schwan (1987)
t	30 μm	Bacon *et al* (2006)
ϕ_0	$0.1 < \phi_0 < 0.4$	Appendix A
ϕ_{p}	$0.1 < \phi_{\mathrm{p}} < 0.4$	Model parameter
Δ	0.1	Model parameter

Table 2. Parameters for equation (2) used to empirically model the dielectric spectrum of liver tissue (from table 1, Gabriel *et al* 1996a). $\varepsilon_\infty = 4.0$ and $\sigma_{\mathrm{s}} = 0.02$ S m^{-1}.

n	$\Delta\varepsilon_n$	τ_n	α_n
1	39	8.84 ps	0.1
2	6000	530.52 ns	0.2
3	5.0×10^4	22.74 μs	0.2
4	3.0×10^7	15.915 ms	0.05

for λ, μ. The parameter values required for equation (2) are given in table 2 for liver (from Gabriel *et al* (1996a)).

4. Results

The dispersion relations for ε' and σ are illustrated in figures 4–11 for $10^4 < f < 10^7$ Hz (plotted as logarithmic values) over a range of parameter values given in table 1 (and noted on each figure) and in comparison with the empirical values fitted by the Cole–Cole relationship for liver tissue (see equation (2) and table 2).

5. Discussion

The model describes the complex permittivity of a tissue as a weighted spatial average of the separate permittivities of conducting and blocking elements. The permittivities of the elements are, in turn, derived from simple geometrical models.

The results shown in figures 4–11 demonstrate a number of important features; the permittivity ε' is relatively strongly dependent on ϕ_0 at the lower frequencies but less sensitive to the values of Δ and ϕ_{p} in the frequency range $10^4 < f < 10^7$ Hz. From figure 4(a), as ϕ_0 increases, ε' decreases. This is likely to be due to increasing dominance of purely conductive pathways in the tissue increase. The model dispersion curves in figures 4(a) and 5(a) assume a different shape to the Cole–Cole fit, as ε' attains a plateau value at lower frequencies for the largest values of ϕ_0 and ϕ_{p}, respectively. From figure 5(a), as ϕ_{p} increases, ε' initially increases ($\phi_{\mathrm{p}} = 0.15$) and then decreases ($\phi_{\mathrm{p}} = 0.25$). Figure 4(b) confirms that σ increases as ϕ_0 increases, the result of more conducting pathways occurring in the tissue. In figure 5(b), σ decreases as ϕ_{p} increases, the result of the tissue impedance being increasingly dominated by capacitive terms as the percolation threshold increases.

Figures 6(a) and (b) show that the model dispersion is relatively insensitive to the value of the parameter Δ in the frequency range $10^4 < f < 10^7$ Hz and for the other parameter

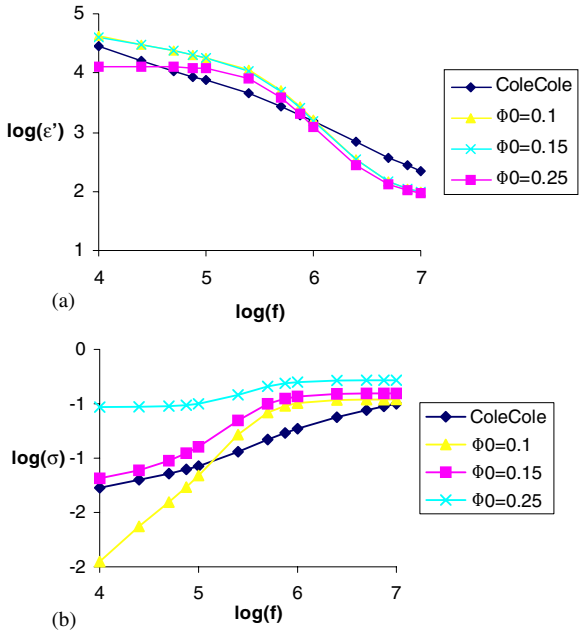

Figure 4. (a) Dispersion for ε' over frequency range $10^4 < f < 10^7$ for $\phi_p = 0.15$, $\Delta = 0.1$ and other parameter values as in table 1. (b) Dispersion for σ over frequency range $10^4 < f < 10^7$ for $\phi_p = 0.15$, $\Delta = 0.1$ and other parameter values as in table 1.

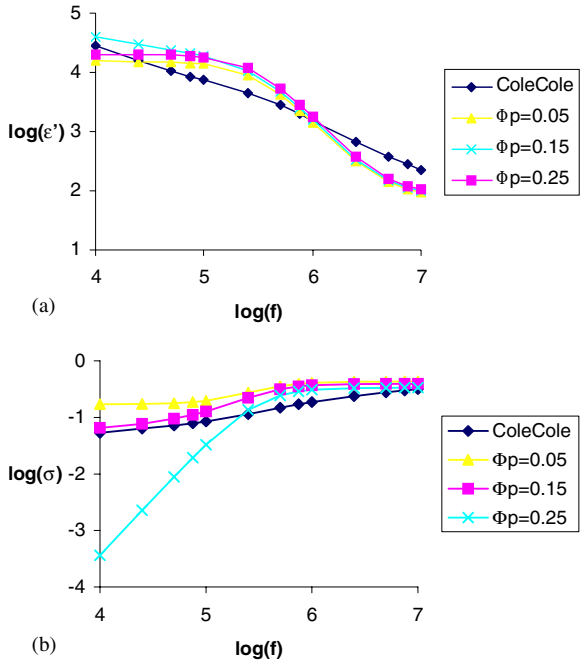

Figure 5. (a) Dispersion for ε' over frequency range $10^4 < f < 10^7$ for $\phi_0 = 0.15$, $\Delta = 0.1$ and other parameter values as in table 1. (b) Dispersion for σ over frequency range $10^4 < f < 10^7$ for $\phi_0 = 0.15$, $\Delta = 0.1$ and other parameter values as in table 1.

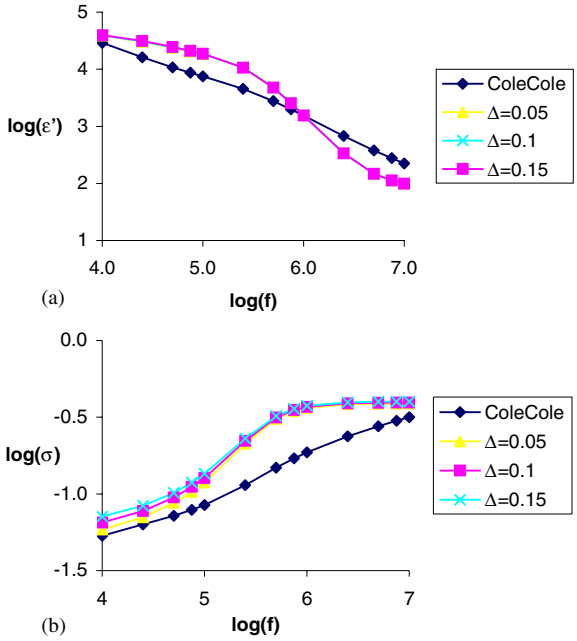

Figure 6. (a) Dispersion for ε' over frequency range $10^4 < f < 10^7$ for $\phi_0 = 0.15$, $\phi_p = 0.15$ and other parameter values as in table 1. (b) Dispersion for σ over frequency range $10^4 < f < 10^7$ for $\phi_0 = 0.15$, $\phi_p = 0.15$ and other parameter values as in table 1.

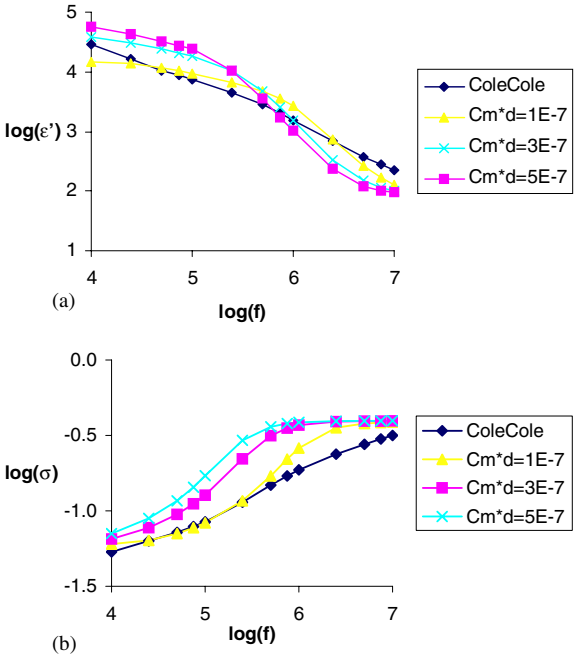

Figure 7. (a) Dispersion for ε' over frequency range $10^4 < f < 10^7$ for $\phi_0 = 0.15$, $\phi_p = 0.15$, $\Delta = 0.1$ and range of C_m values. Other parameter values as in table 1. (b) Dispersion for σ over frequency range $10^4 < f < 10^7$ for $\phi_0 = 0.15$, $\phi_p = 0.15$, $\Delta = 0.1$ and range of C_m values. Other parameter values as in table 1.

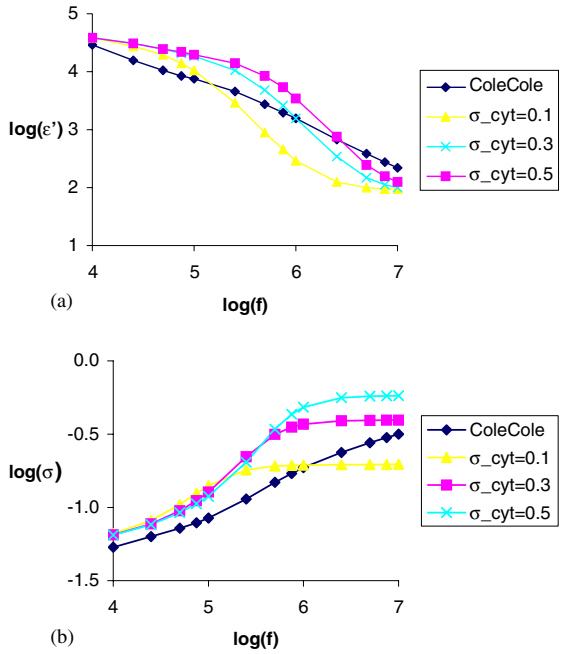

Figure 8. (a) Dispersion for ε' over frequency range $10^4 < f < 10^7$ for $\phi_0 = 0.15$, $\phi_p = 0.15$, $\Delta = 0.1$ and range of σ_{cyt} values. Other parameter values as in table 1. (b) Dispersion for σ over frequency range $10^4 < f < 10^7$ for $\phi_0 = 0.15$, $\phi_p = 0.15$, $\Delta = 0.1$ and range of σ_{cyt} values. Other parameter values as in table 1.

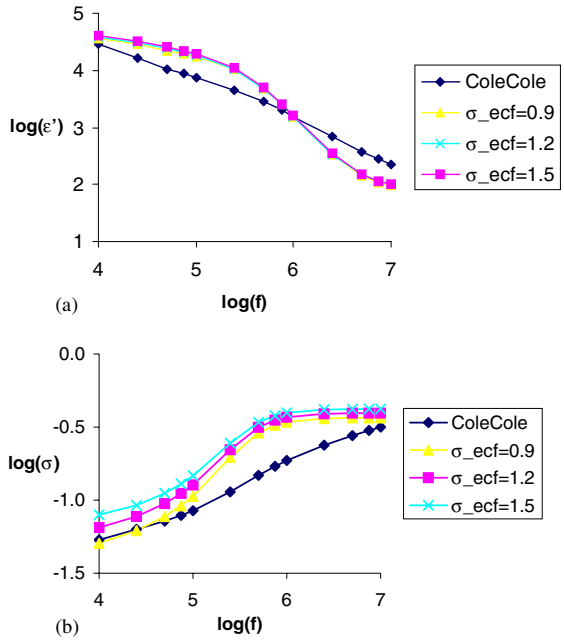

Figure 9. (a) Dispersion for ε' over frequency range $10^4 < f < 10^7$ for $\phi_0 = 0.15$, $\phi_p = 0.15$, $\Delta = 0.1$ and range of σ_{ecf} values. Other parameter values as in table 1. (b) Dispersion for σ over frequency range $10^4 < f < 10^7$ for $\phi_0 = 0.15$, $\phi_p = 0.15$, $\Delta = 0.1$ and range of σ_{ecf} values. Other parameter values as in table 1.

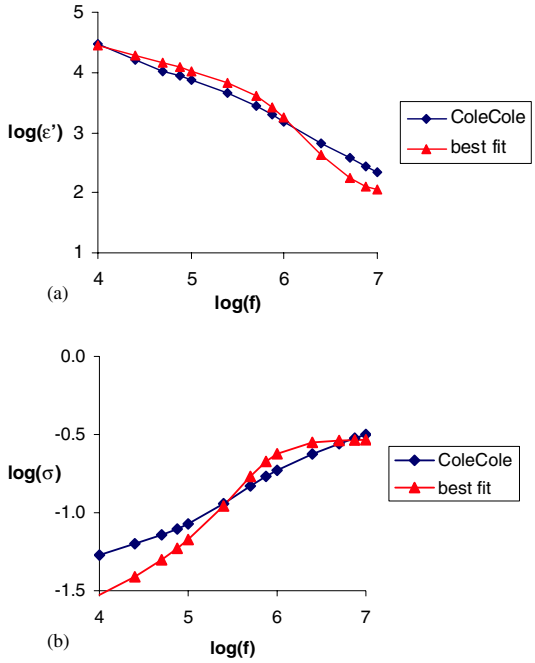

Figure 10. (a) Best fit of model to Cole–Cole dispersion for ε' over frequency range $10^4 < f < 10^7$. $\phi_0 = 0.18$, $\phi_p = 0.2$, $\Delta = 0.1$, $\sigma_{cyt} = 0.2$, $\sigma_{ecf} = 1.2$, $C_m = 0.005$ F m^{-1} and $t = 20$ μm. Other parameter values as in table 1. (b) Best fit of model to Cole–Cole dispersion for σ over frequency range $10^4 < f < 10^7$. $\phi_0 = 0.18$, $\phi_p = 0.2$, $\Delta = 0.1$, $\sigma_{cyt} = 0.2$, $\sigma_{ecf} = 1.2$, $C_m = 0.005$ F m^{-1} and $t = 20$ μm. Other parameter values as in table 1.

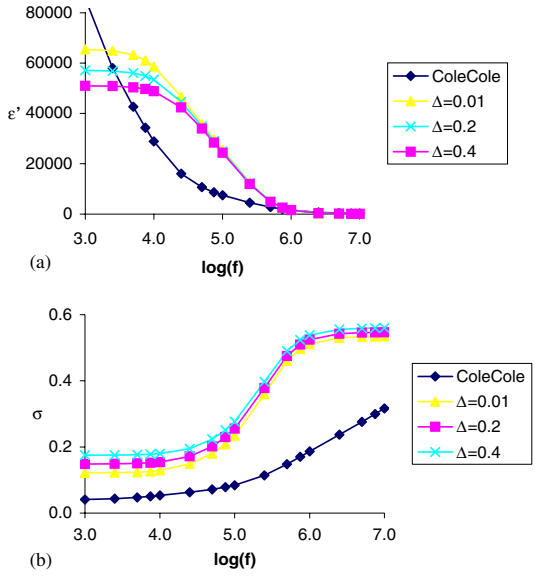

Figure 11. (a) Dispersion for ε' compared to Cole–Cole empirical plot over frequency range $10^4 < f < 10^7$ for different values of Δ, plotted using linear y-axis. $\phi_0 = \phi_p = 0.4$. Other parameter values as in table 1. (b) Dispersion for σ compared to Cole–Cole empirical plot over frequency range $10^4 < f < 10^7$ for different values of Δ, plotted using linear y-axis. $\phi_0 = \phi_p = 0.4$. Other parameter values as in table 1.

values in the ranges noted. However, the dispersion does show a stronger dependence at lower frequencies (see figures 11(a) and (b)), albeit at higher values of ϕ_p and ϕ_0 than is used to match the experimental data.

Figures 7(a) and (b) show the effect of increasing the cell membrane capacitance parameter C_m on the dispersion: ε' increases as C_m increases at lower frequencies, but this trend is reversed at higher frequencies. In figure 7(b), the curves for $\sigma(f)$ converge to a common plateau value as f increases, whereas in figure 8(b), which shows the change of σ with σ_{cyt}, the high frequency plateau value for σ is dependent on σ_{cyt}. Figures 8(a) and 9(a) confirm that ε' is less sensitive to the values of σ_{cyt} and σ_{ecf}. Figure 9(b) also confirms that σ_{ecf} does not affect the value of σ significantly over the range of parameters given. Figures 10(a) and (b) show estimated best-fit curves, achieved by parameter adjustment within experimentally credible ranges, justified in table 1. It is important to note that the experimental data used in this instance are likely to have included contributions from cells other than those found in liver lobules, whereas the model is based on estimates of parameters from liver lobules only. This factor will account for some of the observed differences between experimental data and model predictions.

For the parameter values assumed here, a stronger dependence of ε', σ on the porosity ϕ is noted at the lower frequencies. This trend, and those noted above, reflect the effect that the emergence of conducting pathways in the tissue has on the overall electrical properties in the lower regions of the β-dispersion as, in this frequency regime, the capacitive properties of the membranes offer the highest impedance. The effect on the dispersion of a different underlying geometric description of the elemental conducting or blocking element, here deemed to be a rectangular slab, or a different cell geometry (here assumed to be cubic close-packed) may be studied, and may be based on detailed ultra-structural studies. The 'blocking' geometry is associated with a cellular structure, which comprises both membrane and cytoplasm and is therefore described by both permittivity and conductivity, unlike the Hilfer analysis (1991), where the blocking unit has zero conductivity.

It is also possible to modify the existing model to include a different form for $\lambda(\phi)$ and, for example, to estimate a critical value of ϕ such that $\lambda = \lambda_p$ for larger values of ϕ. The analysis also permits a more complex mathematical treatment, based on the integral equation (4), rather than making the simplifying assumptions that lead to equation (14). Such a treatment might include a more complex distribution function for $\mu(\phi)$—for example, a Gaussian distribution function—but one which was based more closely on experimental measurements.

This analysis is based on an effective mean field treatment of the electric field in the tissue, in which an average induced dipole is taken into account for every cell. The contribution of higher order multi-poles is neglected and each cell is polarized as if it were in an effective homogeneous field. An alternative approach would be to describe the tissue as an inhomogeneous medium with particles (the tissue cells) included in a continuous matrix (the so-called cermet topology). A numerical analysis of this topology, in which the multi-pole moments developed by the ith particle (cell) due to the interactions with other particles are expressed in terms of the particles' dielectric properties, radii and spatial coordinates, is given by Spanoudaki and Pelster (2001). However, previous work (see, for example, Smye (2001)) indicates that higher order multi-pole interactions are not likely to be significant for most biological tissues.

As noted in the introduction, possible applications of the model may include describing the electrical properties of malignant tissue and modelling the behaviour of tissue in which changes in the water content cause changes in ϕ and λ. Assessment of the utility of the model for these clinical applications would need to be preceded by a series of more detailed experimental measurements of ϕ and λ, but if validated, it is also possible that solving the

inverse problem—that is, calculating ϕ, λ from electrical measurements of the tissue sample—may yield a parametric description of tissue, which might then be useful in monitoring changes in tissue over the course of a disease (for example, during tumour progression or response to therapy).

6. Conclusions

The frequency dependence of the conductivity and permittivity of a biological tissue in the β-dispersion has been described by a model, which treats tissue as a porous medium. The analysis uses two parameters, porosity ϕ and percolation probability λ, to describe the geometry of the tissue. These parameters provide a method for capturing the key geometrical features of the tissue that influence electrical properties. In particular, the parameters permit the statistical distribution of features to be described in a way that is more readily appreciated than an *ab initio* mathematical description of the tissue structure. Whilst the model dispersion relation shows broad agreement with data published on liver tissue as an exemplar, further experimental work is required to link this theoretical framework to structural measurements at a cellular level.

Acknowledgments

The assistance and advice of SE Bacon, who undertook the image analysis described in appendix A, is gratefully acknowledged.

Appendix A

In figure 2, the irregular polygonal shapes denote liver cells, the dark circular areas red blood cells and the white area extracellular space. Assuming the two-dimensional representation of the tissue is representative of the three-dimensional distribution of porosity, $\bar{\phi}$ may be estimated from figure 2 as follows:

- The image is digitized and an image-thresholding tool is then applied to the digitized image (Matlab v6.1, The Mathworks Inc.) so that

$$I(n) \text{ set to } 0 \text{ if } I(n) < t \qquad I(n) \text{ set to } 1 \text{ if } I(n) > t$$

  where $I(n)$ denotes the intensity value of the nth pixel (the pixel with the maximum intensity, $n_{\max}$, is set to an intensity value $I(n_{\max})$ of 1) and t is the threshold chosen to achieve maximum visual delineation between the liver cells and extracellular space. The result is shown in figure 12, where black pixels denote liver cells and white denote extracellular space (ignoring the red blood cells).
- From figure 12, the image analysis tool is then used to count the number of white and black pixels, denoted as Wp and Bp respectively, and the ratio Wp/(Wp + Bp) is estimated as 0.24. This gives an estimate of the (three-dimensional) porosity $\bar{\phi}$ as $(0.24)^{3/2} = 0.12$.

The fraction of space occupied by red cells may be measured by a similar technique and in this case was estimated as 0.07 but the effect of red cells is not considered separately in this analysis. λ might also be estimated from this type of image, perhaps based on an analysis of connections between sides of a unit-cell grid.

Figure 12. Image analysis of digitized version of figure 2; thresholding undertaken as described in the text. White pixels denote extracellular space and black pixels denote liver cellular tissue. The total numbers of white and black pixels are denoted by Wp and Bp, respectively, and the ratio Wp/(Wp + Bp) is 0.24 for this image. This gives an estimate of the (three-dimensional) porosity as $(0.24)^{3/2} = 0.12$

Appendix B

In the 'blocking' geometry, it is assumed that there are no spaces between the cells and that the cells are arranged as a closely packed cubic array of cells, each of side t. The total capacitance of the cell C_{cell} is the series combination of the membrane capacitance C_1 and cytoplasm capacitance C_2. Note that owing to the complex permittivity of the cytoplasm these may be complex quantities. They are given by

$$C_1 = \frac{C_{\text{m}}A}{2} \qquad C_2 = \frac{\varepsilon_{\text{cyt}}\varepsilon_0 A}{t}$$

where C_{m} is the membrane capacitance *per unit area* and the factor of 2 is due to there being two membranes (top and bottom of cell). The combined capacitance is then

$$C_{\text{cell}} = \left(\frac{1}{C_1} + \frac{1}{C_2}\right)^{-1} = \frac{\varepsilon_{\text{cell}}\varepsilon_0 A}{t}$$

where it is assumed that $d \gg$ membrane thickness. Substituting and re-arranging gives the expression

$$\varepsilon_{\text{cell}} = \varepsilon_{\text{cyt}}\left(1 + \frac{2\varepsilon_{\text{cyt}}\varepsilon_0}{C_{\text{m}}t}\right)^{-1}$$

where the complex permittivity of the cytoplasm ε_{cyt} is given by

$$\varepsilon_{\text{cyt}} = \varepsilon'_{\text{cyt}} + \frac{\text{i}\sigma_{\text{cyt}}}{2\pi f \varepsilon_0}$$

and $\varepsilon'_{\text{cyt}}$ and σ_{cyt} are the dielectric constant and conductivity of the cytoplasm. Similarly, the complex permittivity of the extracellular fluid is given by

$$\varepsilon_{\text{ecf}} = \varepsilon'_{\text{ecf}} + \frac{\text{i}\sigma_{\text{ecf}}}{2\pi f \varepsilon_0}$$

where ε'_{ecf} and σ_{ecf} are the dielectric constant and conductivity of the extracellular fluid. It is also assumed that $\varepsilon'_{ecf} = \varepsilon'_{cyt}$. The parameter values are given in table 1.

References

Bacon B R, DiBisceglie A M, O'Grady J G and Lake J R 2006 *Comprehensive Clinical Hepatology* 2nd edn (Philadelphia, PA: Elsevier Mosby) p 6

Boned C and Peyrelasse J 1983 Etude de la permittivitie complex d'ellipsoides disperses dans un milieu continu. Analyses theorique et numerique *Colloid. Polym. Sci.* **261** 600–12

Bradbury M G, Smye S W and Brocklebank J T 2001 Measurement of the intercompartmental fluid shifts during haemodialysis in children *Physiol. Meas.* **22** 351–63

Cole K S and Cole R H 1941 Dispersion and absorption in dielectrics: I. Alternating current characteristics *J. Chem. Phys.* **9** 341

Cormack D H 2001 *Essential Histology* 2nd edn (Philadelphia, PA: Lippincott, Williams and Wilkins) pp 323–9

Dissado L A 1990 A fractal interpretation of the dielectric response of animal tissues *Phys. Med. Biol.* **35** 1487–503

Feldman Y, Pazenko A and Ryabov Y 2002 Non-Debye dielectric relaxation in complex materials *Chem. Phys.* **284** 139–68

Foster K R and Schwan H P 1989 Dielectric properties of tissues and biological materials: a critical review *Crit. Rev. Biomed. Eng.* **17** 25–104

Gabriel S, Lau R W and Gabriel C 1996a The dielectric properties of biological tissues: III. Parametric models for the dielectric spectrum of tissues *Phys. Med. Biol.* **41** 2271–93

Gabriel S, Lau R W and Gabriel C 1996b The dielectric properties of biological tissues: II. Measurements in the frequency range 10 Hz to 20 GHz *Phys. Med. Biol.* **41** 2251–70

Gielen F L H, Cruts H E P, Albers B A, Boon K L, Wallinga-de Jonge W and Boom H B K 1986 Model of electrical conductivity of skeletal muscle based on tissue structure *Med. Biol. Eng. Comput.* **24** 34–40

Gowrishankar T R and Weaver J C 2006 Electrical behaviour and pore accumulation in a multicellular model for conventional and supra-electroporation *Biochem. Biophys. Res. Commun.* **349** 643–53

Hanai T, Asami K and Koizumi N 1979 Dielectric theory of concentrated suspensions of shell-spheres, in particular reference to the analysis of biological cell suspensions *Bull. Inst. Chem. Res. Kyoto Univ.* **57** 297–305

Haslund E, Hansen B D, Hilfer R and Nøst B 1994 Measurement of local porosities and dielectric dispersion for a water-saturated porous medium *J. Appl. Phys.* **76** 5473–80

Hilfer R 1991 Geometric and dielectric characterisation of porous media *Phys. Rev.* B **44** 60–75

Landauer R 1978 Electrical conductivity in inhomogeneous media *Electrical Transport and Optical Properties of Inhomogeneous media* ed J C Garland and D B Tanner (New York: American Institute of Physics)

Leeson T S and Lesson C R 1981a *Histology* (Philadelphia, PA: Saunders) p 384

Leeson T S and Lesson C R 1981b *Histology* (Philadelphia, PA: Saunders) p 388

MacDonald J R 1987 Linear relaxation: distributions, thermal activation, structure, and ambiguity *J. Appl. Phys.* **62** R51–62

Paulson K S, Jouravleva S and McLeod C N 2000 Dielectric relaxation time spectroscopy *IEEE Trans. Biomed. Eng.* **47** 510–1517

Pethig R and Kell D 1987 The passive electrical properties of biological systems: their significance in physiology, biophysics and biotechnology *Phys. Med. Biol.* **32** 933–70

Raicu V 1999 Dielectric dispersion of biological matter: model combining Debye-type and 'universal' responses *Phys. Rev.* E **60** 4677–80

Sahimi M 2003 *Heterogeneous Materials: I. Linear Transport and Optical Properties* (New York: Springer) pp 162–4

Smye S W 2001 A mathematical comparison of two models of the electrical properties of biological tissues *Phys. Med. Biol.* **46** 867–77

Spanoudaki A and Pelster R 2001 Effective dielectric properties of composite materials: the dependence on the particle size distribution *Phys. Rev.* B **64** 064205-1–6

Walker D C, Brown B H, Hose D R and Smallwood R H 2000 Modelling the electrical impedivity of normal and premalignant cervical tissue *Electron. Lett.* **36** 1603–4

Wilkinson D, Langer J S and Sen P N 1983 Enhancement of the dielectric constant near a percolation threshold *Phys. Rev.* B **28** 1081–7